

## SUPPLEMENTAL MATERIALS

**Title :** Inflammatory serum factors from aortic valve stenosis patients modulate sex differences in valvular myofibroblast activation and osteoblast-like differentiation

**Authors:** Brandon J. Vogt<sup>1,2,3</sup>, Douglas K. Peters<sup>4</sup>, Kristi S. Anseth<sup>3,4</sup>, Brian A. Aguado<sup>1,2\*</sup>

### **Affiliations:**

<sup>1</sup> Department of Bioengineering, University of California San Diego, La Jolla, CA 92093, USA

<sup>2</sup> Sanford Consortium for Regenerative Medicine, La Jolla, CA 92037, USA

<sup>3</sup> Department of Chemical and Biological Engineering, University of Colorado Boulder, CO 80303, USA

<sup>4</sup> BioFrontiers Institute, University of Colorado Boulder, CO 80309, USA

### **\*Address correspondence to:**

Brian A. Aguado, Ph.D.

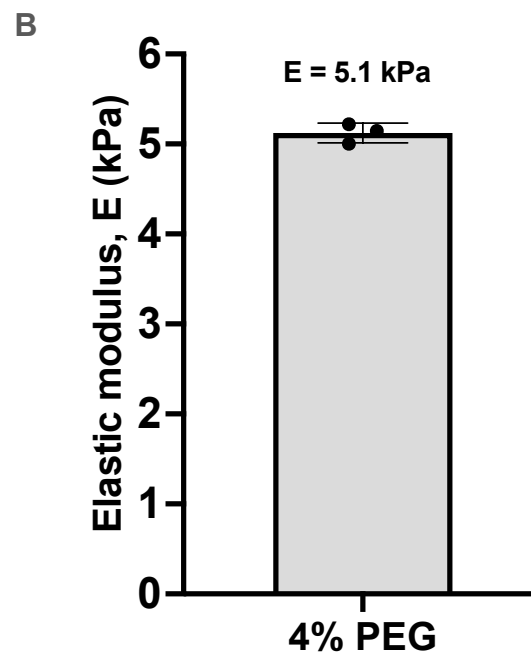
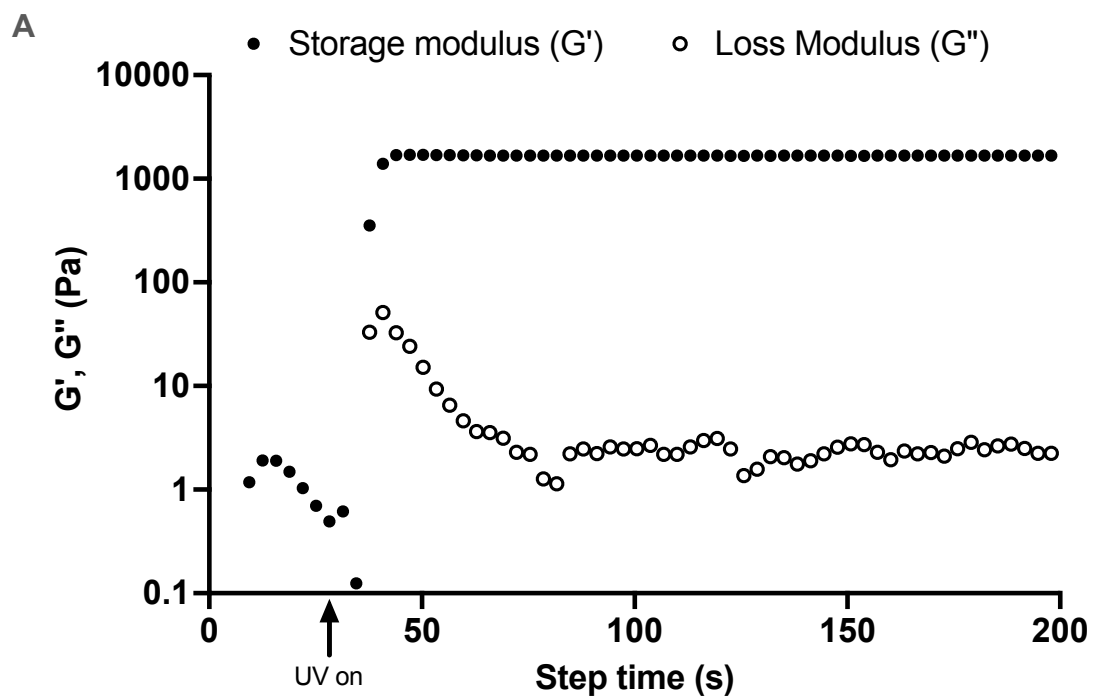
2880 Torrey Pines Scenic Drive

University of California San Diego

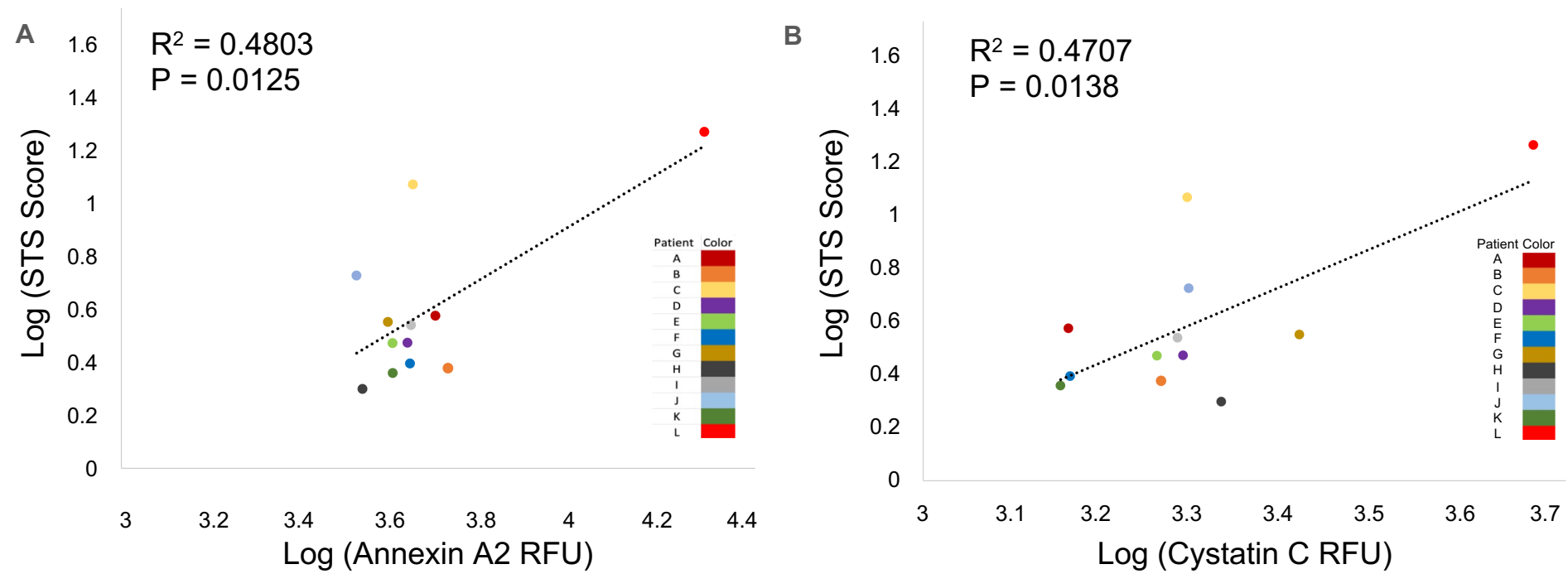
Sanford Consortium for Regenerative Medicine

La Jolla, CA 92037

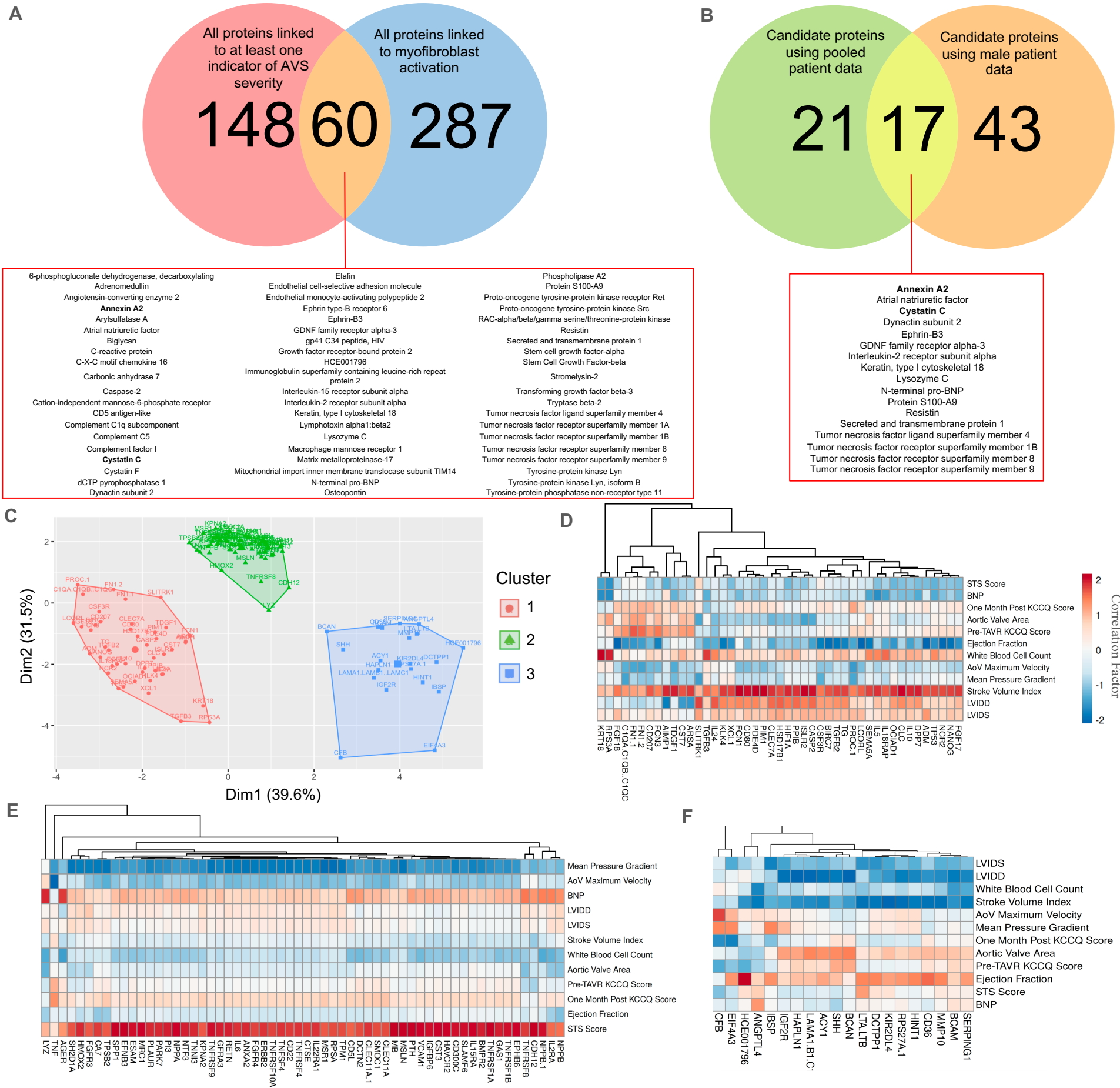
Email: [baguado@eng.ucsd.edu](mailto:baguado@eng.ucsd.edu)



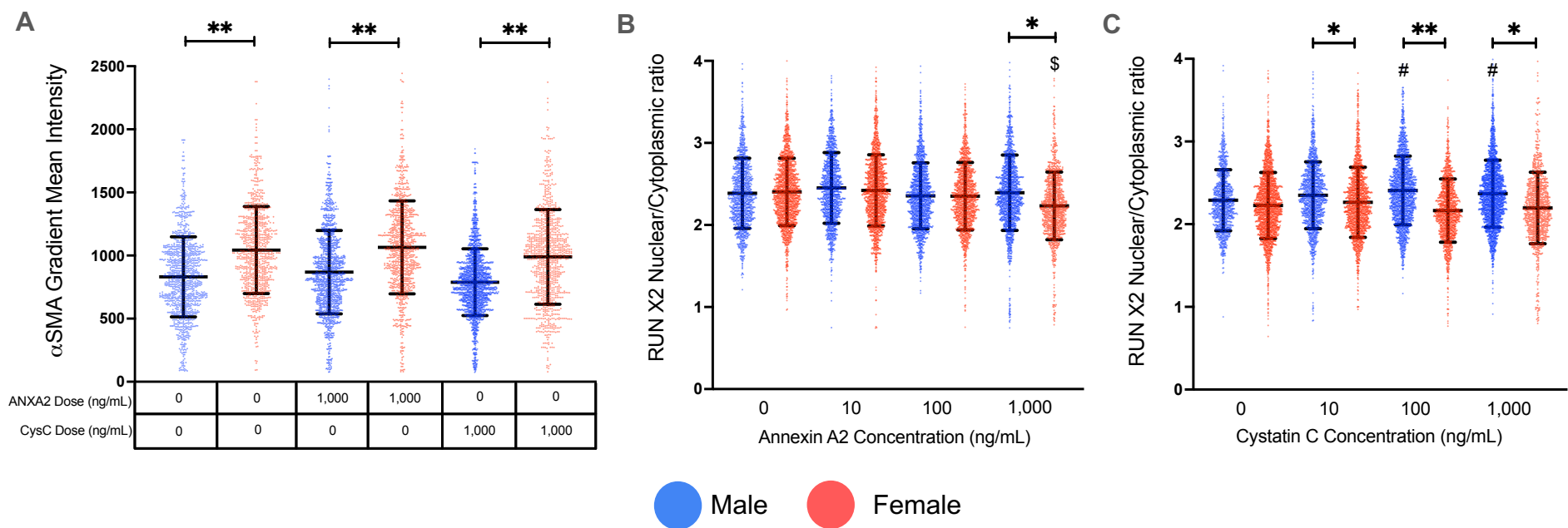
**Supplemental Figure 1.** *Rheological measurements of PEG hydrogels.* (A) Storage and loss moduli of hydrogel precursor solution upon exposure to UV light. N=1 representative measurement shown. (B) Elastic modulus of 4% PEG formulation used to form hydrogels. N=3 measurements, mean  $\pm$  standard deviation shown.



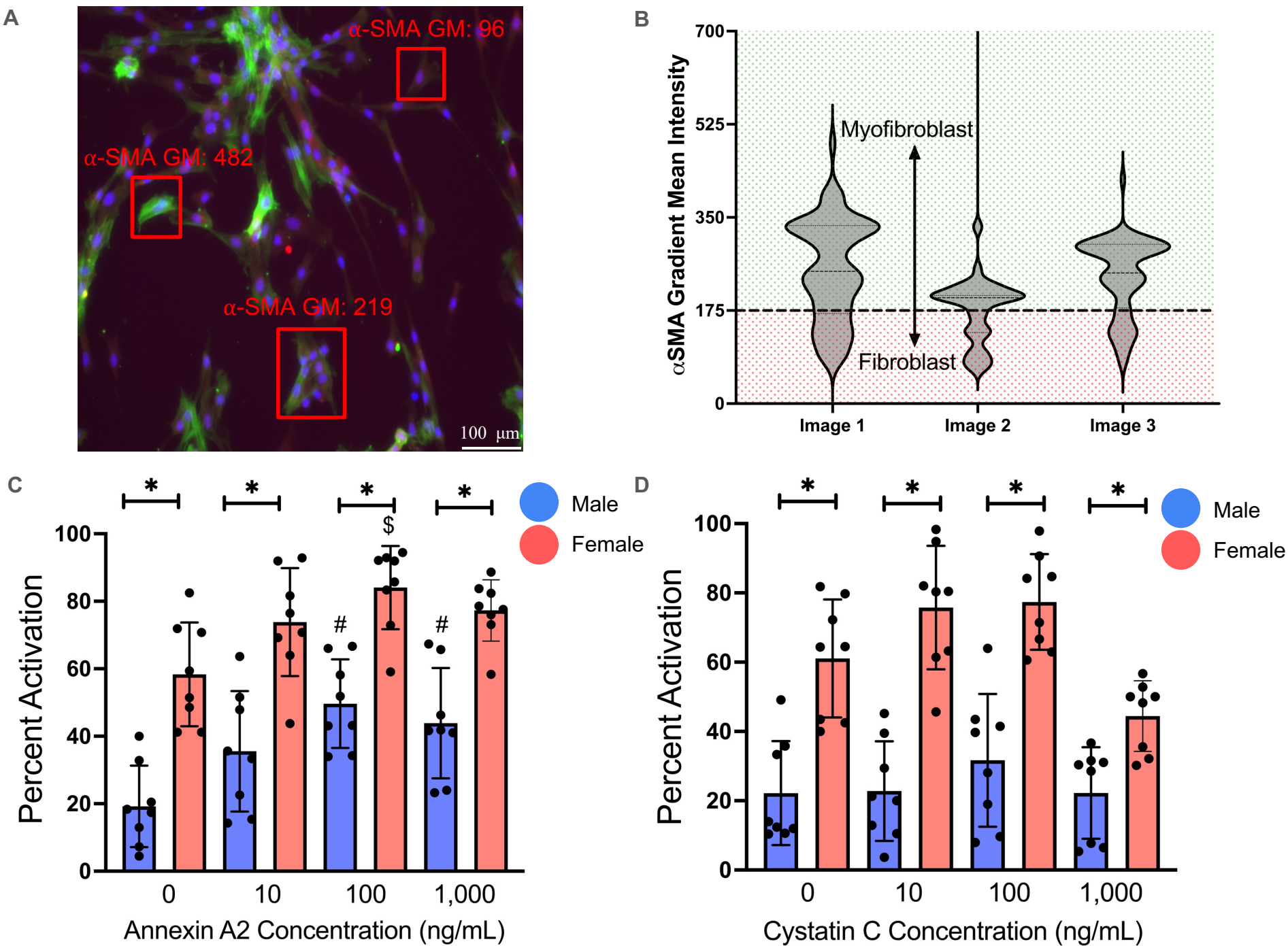
**Supplemental Figure 2.** *Linear regression analysis on the logarithmic transformation of STS score and protein abundance eliminates strong outliers and confirms significant correlations. (A-B)* Correlation plots comparing patient STS score and (A) annexin A2 abundance or (B) cystatin C abundance. Strong outliers were defined as  $Q1 - 3 \cdot IQR$  and  $Q3 + 3 \cdot IQR$  based on  $\log(\text{STS score})$ .  $Q1$  = quartile 1,  $Q3$  = quartile 3, and  $IQR$  = interquartile range.



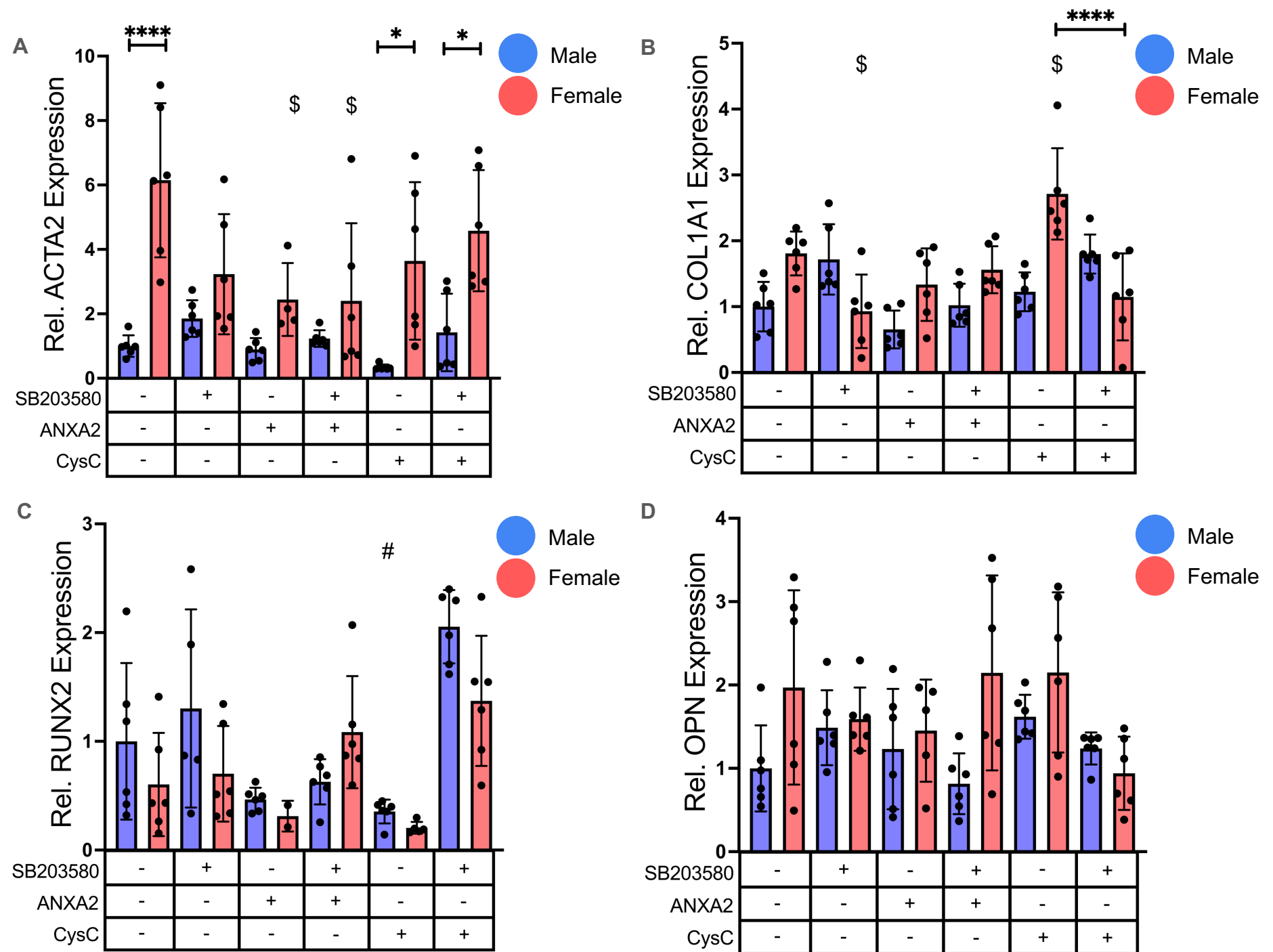
**Supplemental Figure 3. Correlation analysis determines clinically relevant candidate proteins in male patient serum samples** (A) Venn diagram showing the overlap between proteins significantly correlated ( $R > 0.9$ ) with at least one measure of AVS severity and proteins significantly correlated ( $R > 0.75$ ) with myofibroblast activation *in vitro*. (B) Venn diagram showing the overlap between candidate proteins from pooled patient data and male patient data. (C) K-means cluster plot grouping serum proteins significantly correlated ( $R > 0.9$ ) with at least one clinical measure of AVS severity into three clusters. (D-F) Correlation matrices showing (D) cluster 1, (E) cluster 2, and (F) cluster 3 proteins that significantly correlate ( $R > 0.9$ ) with at least one measure of AVS severity.



**Supplemental Figure 4.** VICs cultured on TCPS show minimal changes in myofibroblast activation and osteoblast-like differentiation (A)  $\alpha$ -SMA gradient mean intensity data of VICs treated with either annexin A2 or cystatin C on TCPS. (B-C) RUN X2 nuclear localization data of VICs treated with (B) annexin A2 or (C) cystatin C on TCPS. For all graphs, data is shown as mean  $\pm$  standard deviation with statistical significance determined by one-way ANOVA with Tukey posttests ( $p < 0.0001$ ) and effect size between statistically significant groups measured by the Cohen's d-value indicated by  $** = d > 0.5$ ,  $* = d > 0.2$  for sex differences;  $\# = d > 0.2$  for differences from the male control group;  $\$ = d > 0.2$  for differences from the female control group.



**Supplemental Figure 5.** Quantifying the percentage of VICs activating to myofibroblasts using thresholds for  $\alpha$ -SMA gradient mean intensity confirms annexin A2 and cystatin C increase VIC myofibroblast activation. **(A)** Representative image showing  $\alpha$ -SMA gradient mean (GM) values for individual cell groups. **(B)** Violin plots of three representative images to determine  $\alpha$ -SMA GM threshold. **(C)** Bar graph showing percent activation of VICs treated with annexin A2 and cultured on hydrogels. **(D)** Bar graph showing percent activation of VICs treated with cystatin C and cultured on hydrogels. For immunofluorescent stains: green =  $\alpha$ -SMA; red = RUNX2; blue = DAPI. For all graphs, data is shown as mean  $\pm$  standard deviation with statistical significance determined by one-way ANOVA with Tukey posttests. Statistical significance ( $p < 0.05$ ) is indicated by \* for sex differences; # for differences relative to the male control group; \$ for differences relative to the female control group.



**Supplemental Figure 6.** *Quantitative ACTA2, COL1A1, RUNX2, and OPN gene expression using RT-PCR.* (A) *ACTA2*, (B) *COL1A1*, (C) *RUNX2*, and (D) *OPN* gene expression in male and female VICs cultured on hydrogels and treated with annexin A2, cystatin C, SB203580, or combinations. All gene expression is normalized to male vehicle control. For all graphs, data is shown as mean  $\pm$  standard deviation with statistical significance determined by one-way ANOVA with Tukey posttests. Statistical significance is indicated by \*\*\*\* =  $p < 0.0001$ , \* =  $p < 0.05$  for differences between groups; # =  $p < 0.05$  for differences relative to the male vehicle control; \$ =  $p < 0.05$  for differences relative to the female vehicle control.

**Supplemental Table 1: Primers used for RT-PCR**

<b>Gene</b>	<b>Forward Primer (5'-3')</b>	<b>Reverse Primer (5'-3')</b>
<i>RPL30</i>	AGATTTCTCAAGGCTGGGC	GCTGGGGTACAAGCAGACTC
<i>ACTA2</i>	GCAAACAGGAATACGATGAAGCC	AACACATAGGTAACGAGTCAGAGC
<i>COL1A1</i>	GGGCAAGACAGTGATTGAATACA	GGATGGAGGGAGTTTACAGGAA
<i>RUNX2</i>	AACAACCACAGAACCACAAG	TGACCTGCGGAGATTAACC
<i>OPN</i>	GCGTCTTCTGAGATCAACTG	CACTATACATTCACCAACTAAGC



**Supplemental Table 2: Abbreviations for candidate proteins**

<b>Protein Abbreviation</b>	<b>Full Protein Name</b>	<b>Protein Abbreviation</b>	<b>Full Protein Name</b>
<b>ANXA2</b>	<b>Annexin A2</b>	LYZ	Lysozyme C
ARG1	Arginase-1	MAPK12	Mitogen-activated protein kinase 12
ANF	Atrial natriuretic factor	NBL1	Neuroblastoma suppressor of tumorigenicity 1
CA13	Carbonic anhydrase 13	NPPB	N-terminal pro-BNP
CCL24	C-C motif chemokine 24	NTF3	Neurotrophin-3
<b>CysC</b>	<b>Cystatin C</b>	PES1	Pescadillo homolog
DLL4	Delta-like protein 4	S100A9	Protein S100-A9
DKK3	Dickkopf-related protein 3	PDXK	Pyridoxal kinase
DCTN2	Dynactin subunit 2	CRYZL1	Quinone oxidoreductase-like protein 1
EFNB3	Ephrin-B3	RARRES2	Retinoic acid receptor responder protein 2
FN1	Fibronectin Fragment 3	SECTM1	Secreted and transmembrane protein 1
GFRA3	GDNF family receptor alpha-3	SPHK1	Sphingosine kinase 1
CXCL1	Growth-regulated alpha protein	TAGLN2	Transgelin-2
EHMT2	Histone-lysine N-methyltransferase	TPM4	Tropomyosin alpha-4 chain
IFNL2	Interferon lambda-2	TNFSF4	Tumor necrosis factor ligand superfamily member 4
IL2RA	Interleukin-2 receptor subunit alpha	TNFRSF1B	Tumor necrosis factor receptor superfamily member 1B
IL20RA	Interleukin-20 receptor subunit alpha	TNFRSF8	Tumor necrosis factor receptor superfamily member 8
KRT18	Keratin, type I cytoskeletal 18	TNFRSF9	Tumor necrosis factor receptor superfamily member 9
LRRN3	Leucine-rich repeat transmembrane neuronal protein 3	BTK	Tyrosine-protein kinase BTK